Structural Properties of a Carbon-Nanotube Crystal

J. Tersoff

IBM Thomas J. Watson Research Center, Yorktown Heights, New York 10598

R. S. Ruoff

Molecular Physics Laboratory, SRI International, Menlo Park, California 94025

Carbon nanotubes of uniform size may soon be available in macroscopic quantities. Here we examine the ordered condensed phase of these tubes. As the tube diameter varies, the structural properties show a clear transition between two regimes with qualitatively different behavior. Tubes 10 Å and less in diameter behave as rigid cylinders. For diameters over 25 Å, the tubes flatten against each other under the van der Waals attraction, forming a honeycomb structure. This structure exhibits an anomalous rigidity, which does not decrease as expected with increasing tube diameter. Based on reported tube sizes, both regimes should be experimentally accessible.

PACS numbers: 73.20.Dx

Although carbon fullerenes were first detected and studied as individual molecules, some of their most interesting properties appear in the condensed phase. This may also prove to be true of the recently discovered [1] carbon nanotubes. These typically consist of several nested tubes, each like a graphite sheet bent into a cylinder, with an overall diameter of a few nanometers. Nanotubes have attracted intense interest because of their expected properties, including high strength [2] and unique capillary behavior [3].

Iijima and Ichihashi and Bethune *et al.* [4] showed that it is also possible to make single (unnested) carbon nanotubes of discrete sizes. Because of their van der Waals attraction, such tubes will tend to form close-packed bundles [5]. Thus it may soon become possible to make crystals, consisting of two-dimensionally repeated nanotubes. This material would constitute a new phase of carbon, which would have remarkably anisotropic mechanical, electrical, thermal, and chemical properties. It is a natural candidate for ultrastrong fibers, molecular sieves, and quasi-one-dimensional conductors. However, at present, the only possibility for anticipating these properties is through theoretical calculations [2,3,6–10].

Here we examine the fundamental structural properties of carbon nanotube crystals, finding a rich behavior as the tube diameter is varied. There is a crossover between two distinct regimes, corresponding to small and large tubes, respectively. Moreover, the large-tube regime is characterized by an anomalous rigidity, which does not decrease with decreasing density. For all tube diameters, the crystal contains one-dimensional channels which can accommodate a single atomic row of intercalant atoms. This raises the possibility of useful electronic properties, such as high quasi-one-dimensional conductivity or superconductivity.

The calculations here use a valence-force model to treat the atomic interactions within each tube [11]. The van der Waals interaction between tubes is modeled in the usual way with a 6-12 potential parametrized to describe interlayer forces in graphite [12]. For computational efficiency, these interactions are averaged along the atom columns parallel to the cylinder axis [13].

Because of the hexagonal symmetry of a graphite sheet, its elastic properties are two-dimensionally isotropic, and so the helicity of the tube plays no significant role, a great simplification. We construct an infinitely long tube by bending a graphite sheet around an axis perpendicular to the crystal *a* axis, giving zero helical pitch. The tube is periodically repeated in the two other dimensions, forming a hexagonal lattice. (The finite length of real tubes would necessarily introduce defects into the crystal, but here we consider the ideal case of arbitrarily long tubes.) Only single tubes are considered; nested tubes are generally more rigid, for a given diameter [10].

For each tube diameter D we calculate the crystal structure, relaxing the atomic coordinates until all forces are below 10^{-3} eV/Å. Such strict relaxation is necessary for large tubes because of the subtle competition between elastic and van der Waals forces. Figure 1 illustrates the resulting structures. Figure 1(a) shows a cross section of the condensed phase of 10 Å tubes, while Fig. 1(b) shows a section for 40 Å tubes. These are strikingly different. Tubes with 10 Å diameters remain almost perfectly cylindrical, while 40 Å tubes are flattened against each other under the van der Waals interaction, forming a honeycomb structure. Similar distortions have actually been observed for pairs of tubes [10]. In either case there are one-dimensional channels at the points where three tubes meet. The size of these channels is analyzed below, and is generally suitable for a single atomic row of dopant atoms.

The progression from rigid cylinders to hexagons is shown in Fig. 1(c). For $D \geq 30$ Å, the flattening is clearly visible. For $D = 20$ Å, the flattening is only visible if a reference circle is superimposed on the figure. The deviations from a perfect cylinder are barely detectable in this manner for $D = 15$ Å, and are invisible
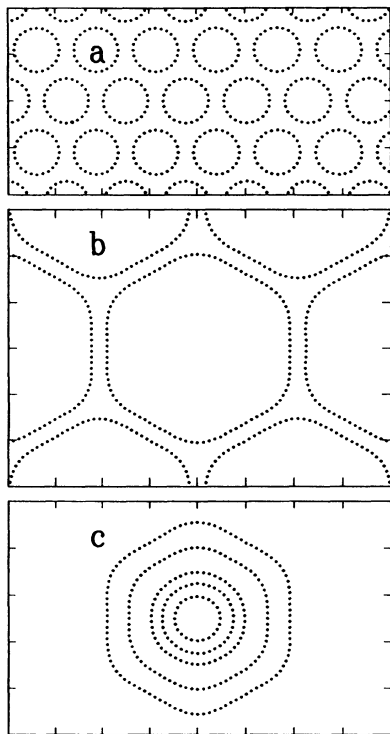
FIG. 1. Calculated structure of nanotube crystals, shown in cross section. Dots are carbon atoms, not all in the same plane. Tic marks are at 10 Å intervals. (a) $D = 10$ Å. (b) $D = 40$ Å. (c) Superposed images of one tube from each of the following crystals: $D = 10, 15, 20, 30$, and 40 Å.

FIG. 2. Calculated structural properties of nanotube crystals, plotted vs tube diameter D. Circles are numerical calculations, dotted lines are analytic results in small-tube limit, and solid lines are analytic results in large-tube limit; see text. (a) Lattice constant L. (b) Cohesive energy of crystal, relative to free tubes. (c) Elastic modulus $M = (c_1 + c_2)/2$.

to the eye for smaller D. Thus we anticipate that a crossover occurs, from small-tube to large-tube behavior, for $D \sim 15$–20 Å. This is confirmed below.

Our results for the structural properties are summarized in Fig. 2. Figure 2(a) gives the zero-pressure lattice constant L for the hexagonal lattice of tubes, as a function of tube diameter D. (For a tube with a circumference of N cells of size $a = 2.46$ Å, the diameter is $D = Na/\pi$.) Figure 2(b) shows the cohesive energy of the solid, i.e., the energy needed to separate it into noninteracting tubes, versus tube diameter. Finally, Fig. 2(c) shows the calculated elastic modulus $M = (c_{11} + c_{12})/2$, the two-dimensional analog of the bulk modulus.

Both the cohesive energy and the compressibility exhibit nonmonotonic behavior, which is highly counterintuitive. The compressibility is particularly anomalous. The density is inversely proportional to the tube diameter; and one expects any given material to become softer as its density decreases. Instead, this material first becomes stiffer, then softer, and finally reaches a value independent of further decrease in density. It is important to understand this behavior—not only is it fascinating, but it bears directly on possible applications. For example, strong fibers composed of carbon nanotubes would in practice probably be embedded in a matrix of some more
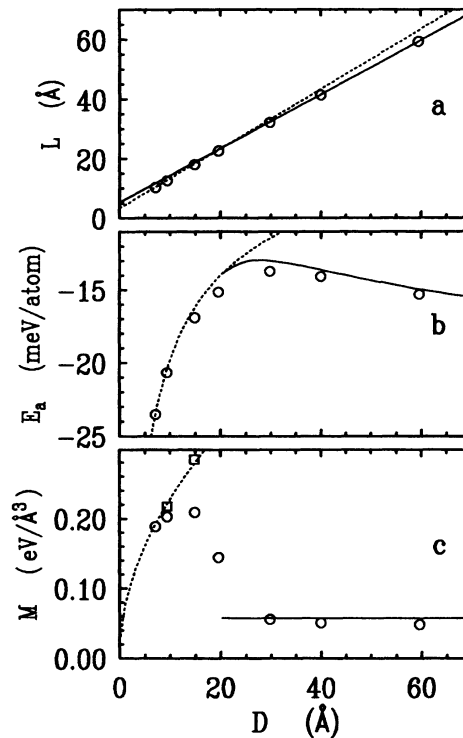
plastic substance. The cohesive energy of the nanotubes would control their tendency to unbind and disperse in the matrix. Their elastic moduli would determine whether stresses are born primarily by the tubes or by the matrix. We therefore seek to understand the peculiar behavior in detail.

The small-diameter behavior may be understood as follows. Consider two cylinders oriented parallel to the z axis, with their axes lying in the y-z plane. If the interaction per unit area between two graphite planes at separation y is $-V(y)$, the interaction energy per length of tube will be

$$E(b) \approx - \int V(b + x^2/R)\, dx = -U(b)R^{1/2}, \quad (1)$$

where $U(b) \equiv \int V(b + \eta^2)\, d\eta$, and $R = D/2$ is the tube radius.

The minimum-energy separation b_0 is seen to be independent of D, so the lattice constant is

$$L = D + b_0. \quad (2)$$

With our treatment of the van der Waals interaction [12,13], $b_0 = 3.42$ Å. This simple parameter-free prediction for the limiting behavior is shown as a dotted line in Fig. 2(a), and agrees very well with the full calculation for $D \le 20$ Å.

The number of atoms per length of tube is $2\pi R/A_a$, where $A_a = 2.62$ Å^2 is the area per atom. Then from Eq. (1) the cohesive energy *per atom* (E_a) is

$$E_a = -U_0 A_a/2\pi\sqrt{R}, \qquad (3)$$

where $U_0 \equiv U(b_0)$. This function is compared with the full calculation in Fig. 2(b) (dotted line), where it is seen to accurately describe the energy for $D \lesssim 20$ Å, with a fitted value of $U_0 = 106$ meV Å$^{-3/2}$.

The elastic properties of this material are highly anisotropic. In the direction along the tube axis, the material is extremely rigid [2], since any distortions are analogous to in-plane distortions of graphite. As with graphite, we expect the stiffness in the strong direction to be less of an issue than interlayer interactions. The tubes are most easily distorted perpendicular to their axis, and any mechanical failure occurs most easily *between* tubes.

We therefore focus on the elastic constant which is analogous to the bulk modulus, but for deformations in the plane perpendicular to the tube axis. This modulus is $M \equiv V^{-1}A^2d^2E/dA^2 = (c_{11} + c_{12})/2$, where V and A are the volume and cross-sectional area, and E is the energy. Using $A = L^2\sqrt{3}/2$ and Eqs. (1) and (2) give

$$M \propto D^{1/2}. \qquad (4)$$

In Fig. 2(c), we see that this relationship is accurately obeyed if the tubes are held rigidly cylindrical (squares). However, the full calculation is close to the rigid-tube behavior only for $D \lesssim 10$ Å. For $D \gtrsim 15$ Å, the material is considerably less stiff than the rigid-tube model predicts, indicating that distortion of the tubes already plays a role in this size range.

Thus the behavior for small D is relatively simple, and can be understood in terms of the van der Waals interaction of rigid cylinders. The behavior at large D is considerably more complex, because the shape of the tube varies with D and with pressure. In the limit of a contact interaction, each tube consists of six flat facets, connected by rounded corners, each of which corresponds to one-sixth of a cylinder whose radius is independent of D. This idealized shape is an excellent description of the full calculation, Fig. 1(b), and we use it as a variational model in the calculations that follow.

The cohesive energy per unit length of tube of the solid (relative to isolated tubes) can then be written as

$$E = -2\pi(R - \rho)\gamma - U_0\sqrt{\rho} + \pi(\rho^{-1} - R^{-1})c_0. \qquad (5)$$

Here ρ is the radius of curvature of the corner, 2γ is the energy required to separate a graphite bilayer, and $2\pi(R - \rho)$ is the total contact area of flat regions per tube length; so the first term in Eq. (5) represents the van der Waals attraction of the faces, and the second term is the attraction of the rounded corners [cf. Eq. (1)]. The elastic constant for bending the graphite sheet is c_0, so the elastic energy per unit area is $c_0/2\rho^2$, over a total circumference of $2\pi\rho$. From this we must subtract the elastic energy of the free-tube reference state, giving the third term in

Eq. (5). With the model used here, $\gamma = 7.6$ meV/Å^2 and $c_0 = 1.02$ eV (close to the value inferred from experiment [11]). Solving Eq. (5) numerically gives $\rho_0 = 10.15$ Å.

With a little geometry, one can show that the lattice constant (i.e., the distance between opposite faces of a tube, plus the tube separation b_0) is

$$L = \left(\pi/2\sqrt{3}\right)D + \left(2 - \pi/\sqrt{3}\right)\rho + b_0. \qquad (6)$$

Substituting the values given above for ρ_0 and b_0 yields the zero-pressure lattice constant: $L_0 = 0.91D + 8.7$ Å. This is compared with the results of the full calculation in Fig. 2(a), where it is seen to give a highly accurate description of the lattice constant for tube diameters of 20 Å and above.

The cohesive energy per atom is obtained by substituting ρ_0 into Eq. (5), and dividing by the number of atoms per unit length, $2\pi R/A_a$ [as for Eq. (3)], giving

$$\frac{E_a}{A_a} = \left(\frac{c_0}{2\rho_0 R} - \gamma\right)\left(1 - \frac{\rho_0}{R}\right) - \frac{U_0\sqrt{\rho}}{2\pi R}. \qquad (7)$$

In Fig. 2(b), we see that this provides a good description of the binding energy for the entire range $R > \rho_0$ where the assumed shape is applicable. Both Eq. (3) and Eq. (7) are upper bounds for the energy, since they use model shapes rather than the exact shape, but they are rather accurate, with a maximum error of 5%–10% in the crossover region $D \sim 20$–30 Å.

We can obtain the compressibility modulus M in the large-tube limit using Eq. (5) for the energy, and changing the independent variable from ρ to L using Eq. (6). The result is

$$M = \pi\sqrt{3}\left(2\sqrt{3} - \pi\right)^{-2}\left(c_0\rho^{-3} + U_0/8\pi\rho^{3/2}\right). \qquad (8)$$

In equilibrium at zero pressure, $\rho = \rho_0$, so M is a constant, independent of the tube diameter. This behavior is clearly seen in Fig. 2(c). Evaluating Eq. (8) gives a large-tube modulus $M = 58$ meV/Å$^3 = 9.3$ GPa, in good agreement with the full calculation. Thus the nanotube solid has the remarkable property that, as it becomes less dense (due to larger tube diameter), the rigidity does not decrease; it remains constant, albeit at a rather small value.

The modulus is also highly nonlinear. Under compression, ρ decreases [Eq. (6)], and so the modulus rapidly increases [Eq. (8)]. For example, for 40 Å tubes, even a 1% linear compression gives a 20% decrease in ρ, and hence a factor of 2 increase in the modulus M. With increasing compression, the modulus will eventually become so high that other modes of deformation become significant, cutting off the divergence in modulus as $\rho \to 0$.

Both graphite and condensed C_{60} can be doped with alkali or other atoms, and the resulting electronic properties (including superconductivity) have been the subject of intense interest. Graphite forms intercalation compounds [14] with two-dimensional sheets of dopant atoms, while in the C_{60} crystal dopants are dispersed in a three-dimensional arrangement [15].

The nanotube crystal should also accommodate electronic doping, but with an interesting difference. In this case, rather than a two- or three-dimensional arrangement, the dopants could form one-dimensional chains in the channels which are present wherever three tubes meet. (These channels are clearly visible in Fig. 1.)

Using the model developed above, the size of these channels is

$$d = b_0/\sqrt{3} + \rho\left(2/\sqrt{3} - 1\right), \qquad (9)$$

measured from the center of the channel to the nearest C. For the large tubes $\rho = \rho_0$, giving $d = 3.5$ Å. This is easily large enough to accommodate even Cs atoms [14]. For small tubes $\rho = D/2$. Even for $D \sim 7$ Å, Eq. (9) gives $d = 3.05$ Å, large enough to accommodate Li or K without any need to distort the channel.

Moreover, for large tubes the energy depends only to second order on the size of the channel, so the channel could easily expand to accommodate larger intercalants. Thus it might be possible to form linear chains of AsF_5, which when intercalated into graphite gives an in-plane room-temperature conductivity greater than copper. At the other extreme, the attractive interaction with smaller intercalant atoms might actually lead to a *shrinking* of the channel, giving the surprising and counterintuitive result that *adding*, e.g., Li atoms would result in a *reduction* of the lattice constant. In contrast, both graphite and C_{60} are always expanded by the introduction of dopants.

In conclusion, an ordered crystal of carbon nanotubes is predicted to exhibit fascinating structural properties. These include a crossover between two distinct regimes of behavior with tube size; an anomalous rigidity for large tubes; and channels which may neatly accommodate one-dimensional chains of dopants.

[1] S. Iijima, Nature (London) **354**, 56–58 (1991).
[2] G. Overney, W. Zhong, and D. Tomanek, Z. Phys. D **27**, 93 (1993).
[3] M. R. Pederson and J. Q. Broughton, Phys. Rev. Lett. **69**, 2689 (1992); S. Iijima and T. Ichihashi, Nature (London) **363**, 603 (1993).
[4] S. Iijima and T. Ichihashi, Nature (London) **363**, 603–605 (1993); D. S. Bethune, C. H. Kiang, M. S. de Vries, G. Gorman, R. Savoy, J. Vazquez, and R. Beyers, Nature (London) **363**, 605–607 (1993).
[5] S. N. Song et al., Phys. Rev. Lett. **72**, 697 (1994).
[6] J. W. Mintmire, B. I. Dunlap, and C. T. White, Phys. Rev. Lett. **68**, 631 (1992).
[7] D. H. Robertson, D. W. Brenner, and J. W. Mintmire, Phys. Rev. B **45**, 12 592 (1992).
[8] R. A. Jishi, M. S. Dresselhaus, and G. Dresselhaus, Phys. Rev. B **47**, 16 671 (1993), and references therein.
[9] J. C. Charlier and J. P. Michenaud, Phys. Rev. Lett. **70**, 1858 (1993).
[10] R. S. Ruoff, J. Tersoff, D. C. Lorents, S. Subramoney, and B. Chan, Nature (London) **364**, 514 (1993).
[11] J. Tersoff, Phys. Rev. B **46**, 15 546 (1992); Phys. Rev. Lett. **61**, 2879 (1988).
[12] L. A. Girifalco and R. A. Ladd, J. Chem. Phys. **25**, 693 (1956).
[13] The averaging of the van der Waals interactions along the atom columns parallel to the cylinder axis results in a slightly expanded interlayer separation for graphite, because the lattices cannot nest in perfect registry. This is ideal for modeling tubules, where registry is not expected, especially given the helical structure of real nanotubes. (Registry has been observed for nested tubes, but here our concern is with side-by-side tubes, where the geometry is even less favorable for registry.)
[14] M. S. Dresselhaus and G. Dresselhaus, Adv. Phys. **30**, 139 (1981).
[15] R. M. Fleming et al., Nature (London) **352**, 787 (1991); O. Zhou et al., Science **255**, 833 (1992).